doi:10.1093/brain/awp042 Brain 2009: 132; 1210–1220 | 1210

BRAIN
A JOURNAL OF NEUROLOGY

In vivo measurement of axon diameter distribution in the corpus callosum of rat brain

Daniel Barazany,[1] Peter J. Basser[2] and Yaniv Assaf[1]

1 Department of Neurobiology, The George S. Wise Faculty of Life Sciences, Tel Aviv University, Tel Aviv, Israel
2 Section of Tissue Biophysics and Biomimetics, The National Institute of Child Health and Human Development, The National Institutes of Health, Bethesda, MD, USA

Correspondence to: Yaniv Assaf,
Department of Neurobiology,
The George S. Wise Faculty of Life Sciences,
Tel Aviv University, Tel Aviv, Israel
E-mail: asafyan@zahav.net.il

Here, we present the first *in vivo* non-invasive measurement of the axon diameter distribution in the rat corpus callosum. Previously, this measurement was only possible using invasive histological methods. The axon diameter, along with other physical properties, such as the intra-axonal resistance, membrane resistance and capacitance etc. helps determine many important functional properties of nerves, such as their conduction velocity. In this work, we provide a novel magnetic resonance imaging method called AxCaliber, which can resolve the distinct signatures of trapped water molecules diffusing within axons as well as water molecules diffusing freely within the extra-axonal space. Using a series of diffusion weighted magnetic resonance imaging brain scans, we can reliably infer both the distribution of axon diameters and the volume fraction of these axons within each white matter voxel. We were able to verify the known microstructural variation along the corpus callosum of the rat from the anterior (genu) to posterior (splenium) regions. AxCaliber yields a narrow distribution centered ~1 μm in the genu and splenium and much broader distributions centered ~3 μm in the body of the corpus callosum. The axon diameter distribution found by AxCaliber is generally broader than those usually obtained by histology. One factor contributing to this difference is the significant tissue shrinkage that results from histological preparation. To that end, AxCaliber might provide a better estimate of the *in vivo* morphology of white matter. Being a magnetic resonance imaging based methodology, AxCaliber has the potential to be used in human scanners for morphological studies of white matter in normal and abnormal development, and white matter related diseases.

Keywords: MRI; brain; corpus callosum; axon diameter distribution; diffusion

Abbreviations: ADC = apparent diffusion coefficient; ADD = axon diameter distribution; CHARMED = Composite Hindered and Restricted Model of Diffusion; DTI = diffusion tensor imaging; DWI = diffusion weighted imaging; EPI = echo planar imaging; FA = fractional anisotropy

Introduction

The inner diameter of axons is an important structural/morphological property of white matter fascicles. The axon diameter along with other physical properties, such as the intra-axonal resistance, membrane resistance and capacitance etc. helps determine many important functional properties of nerves, such as their conduction velocity (Hursh, 1939; Tasaki, 1943; Waxman, 1980; Ritchie, 1982; Waxman *et al*., 1995). Thus, the axon diameter distribution (ADD) is related to the rate of information transfer of a nerve bundle or fascicle. By interference, the distribution of axon diameters in different white matter fascicles within the CNS and PNS

Received August 18, 2008. Revised January 29, 2009. Accepted February 2, 2009.

helps determine the performance of various pathways that they mediate (Waxman, 1980; Waxman *et al*., 1995; Olivares *et al*., 2001).

The fibre composition of white matter regions is determined within the first few years of life through the myelination process. It is evident that abnormal development of the white matter itself or of the cortex will influence axon properties in white matter fascicles. For instance, it is suspected that the diameter distribution of axons in the corpus callosum is altered in autism (Piven *et al*., 1997; Hughes, 2007), dyslexia (Njiokiktjien *et al*., 1994), and even in schizophrenia (Randall, 1983; Rice and Barone, 2000). Moreover, the axon diameter distributions were found to change following exposure to alcohol (Livy and Elberger, 2008) and other toxic drugs. As structure and function are strongly linked in the brain, the measurement of a local structural property is useful in exploring the development of CNS, the effect of neurological diseases, and the correlation of the structural properties with functional and cognitive abilities.

The ADD is traditionally measured using invasive and destructive histological procedures such as electron microscopy and therefore suffers from the limitations of histological procedures: the need to work on post mortem tissue, artifacts caused by fixation and cutting (tissue disintegration, fracturing and shrinkage) (Virtanen *et al*., 1984), and the possibility of sampling and studying only small tissue regions (fields of view <0.1 mm). As a consequence, the relevance of histological findings to *in vivo* white matter is limited and such histological analysis should not be viewed as a 'gold standard'. In addition, histological procedures preclude performing developmental studies (on the same subject or animal). Finally, surgically extracting and preparing brain tissue from small rodents such as mice and rats is extremely challenging, often resulting in significant tissue damage.

Recently, a diffusion MRI based methodology, AxCaliber, was proposed to measure the ADD of white matter structures on a voxel by voxel basis (Assaf *et al*., 2008). AxCaliber uses diffusion weighted MRI data along with a model of intra- and extra-axonal water diffusion to infer the ADD within a pack of nerve axons (Assaf *et al*., 2004, 2008; Assaf and Basser, 2005). Specifically, the model assumes that within axons water diffusion is restricted by the surrounding axonal and myelinated membranes, whereas outside the axons, water diffusion is relatively free or hindered (Assaf *et al*., 2004; Assaf and Basser, 2005). By varying both the diffusion time and the diffusion weighting, one can estimate the ADD that represents the best fit of the analytical model to the experimental magnetic resonance data (Assaf *et al*., 2008). Using this framework, three properties can be inferred: the volume fraction of the axonal compartment (i.e. axonal density), the extra-axonal diffusivity, and the axon diameter distribution. The latter can be estimated either by using a pre-defined parametric probability distribution (e.g. a γ-distribution) (Assaf *et al*., 2008) or by using a non-parametric approach (Assaf and Basser, 2007). AxCaliber was previously applied to measure the ADD of excised neuronal tissue (Assaf *et al*., 2008).

In this work, we applied AxCaliber to measure, for the first time, ADD of the rat's corpus callosum *in vivo*. The corpus callosum is the largest neuronal fibre pathway in the brain, which mediates sensory and cognitive information transfer between the two hemispheres. As the structure connects different regions between hemispheres (e.g. sensory-motor regions and high cognitive performance regions), the architectural and structural features of the white matter can vary significantly from the anterior to posterior portions (Aboitiz *et al*., 1992; Olivares *et al*., 2000, 2001; Aboitiz and Montiel, 2003). Histological studies showed that fibres that connect the sensory-motor and visual regions require fast transmission and that a significant portion of these axons have a large diameter ($>3\,\mu$m). Other regions more related to higher cognitive functions; however, exhibit smaller axon diameters with a narrow distribution. There are many known callosal disorders related to abnormal development of the corpus callosum (Kamnasaran, 2005; Aboitiz and Montiel, 2003). In addition, the size of the structure varies between different groups (e.g. males versus females, left handed versus right handed, etc.) (Aboitiz *et al*., 1992; Olivares *et al*., 2000; Olivares *et al*., 2001; Aboitiz and Montiel, 2003). However, despite these drawbacks, within the scope of this paper we use this brain region as a model system for white matter tissue. The corpus callosum is optimal for implementation of AxCaliber *in vivo* as the fibres alignment with respect to the scanner can be easily determined. Therefore, we demonstrate how MRI can estimate useful structural features of this structure.

This article will describe the ability of AxCaliber to distinguish among white matter regions with different ADDs in the corpus callosum. In addition, we will discuss the relationship among AxCaliber measurements, histological analysis, and the traditional MRI-based white matter parameters (e.g. the fractional anisotropy).

Methods

Animal preparations

Three male 4-month-old Wistar rats were anesthetized with $\sim$2% isoflurane in oxygen throughout the MRI experiments. Body temperature was monitored and maintained at 38°C with a warm water circulation system. The respiratory rate was monitored with a pneumatic sensor placed under the abdomen of each rat.

MRI experiments

MRI was performed on a 7T/30 MRI scanner (Bruker, Germany) equipped with a gradient system with a maximal gradient strength of 400 mT/m. For excitation we used a body-coil (outer/inner diameter of 112/72 mm) and a surface coil (10 mm diameter) as a receiver.

The AxCaliber experimental protocol consisted of a series of diffusion-weighted stimulated-echo echo-planar imaging (EPI) acquisitions with the following parameters: TR/TE = 1500/23 ms, $\delta = 3.2$ ms, $G_{max} = 282$ mT/m, 16 diffusion gradient increments (linearly from 0 to 282 mT/m), 12 averages and four EPI shots. The maximal b-value (at the longest diffusion time, see below) was 5180 s/mm^2. The field of view was 16 mm^2, the matrix size was 128×96 (reconstructed to 128×128) with a resolution of 0.125×0.125 mm^2 for the final images.

The diffusion gradients were applied only along the x-direction, which is perpendicular to the fibres within the corpus callosum in the mid-sagittal plane. The experiment was repeated for five different diffusion times: 11, 20, 30, 60 and 100 ms. Images were acquired in

the sagittal plane with seven 1.8 mm thick slices and no gap between slices. Only the mid-sagittal slice was analysed where the diffusion gradient direction is exactly perpendicular to the fibres. The entire diffusion weighted imaging (DWI) dataset consisted of 80 images per slice acquired in 1.5 h.

In addition to the AxCaliber dataset, we also acquired a diffusion tensor imaging (DTI) dataset with an DWI EPI sequence: TR/TE = 4000/30 ms, $\Delta/\delta = 15/4$ ms, measured at 15 non-collinear gradient directions with a *b*-value of 1000 s/mm^2. The DWIs were acquired in the sagittal plane with seven 1.8-mm thick slices and no gap between slices, with a field of view of 16×12 mm^2 with a matrix of 96×96 (reconstructed to 128×128) with a reconstructed image resolution of 0.125×0.093 mm^2, two averages and four EPI shots. All diffusion scans were done with respiratory gating to reduce the effects of respiratory motion.

For anatomical reference, we acquired proton density and T_2-weighted images using a multi-spin multi-echo sequence with the following parameters: TR = 2000 ms with two different effective TE, 12 ms and 63 ms for proton density and T_2-weighted images, respectively; field of view of 32×32mm^2; and a matrix size of 256×256, which yielded a spatial resolution of 0.125×0.125mm^2, with two averages.

AxCaliber analysis

AxCaliber MRI extends the composite hindered and restricted model of diffusion (CHARMED) MRI framework (Assaf *et al*., 2004; Assaf and Basser, 2005). In general, the CHARMED framework combines contributions of hindered and restricted diffusion arising from the extra- and intra-axonal spaces, respectively. As a consequence, different properties of the intra-axonal space, such as axonal density and orientation, could be inferred. The ADD was originally set within CHARMED to a known averaged distribution of fibres in brain tissue to limit computational complexity (Assaf *et al*., 2004; Assaf and Basser, 2005). In contrast to CHARMED, AxCaliber is designed to measure the ADD but not the axon orientation (which is assumed to be known using other methods). In AxCaliber, diffusion gradients are presumed to be applied perpendicular to the fibre direction (Assaf *et al*., 2008). The multi-diffusion time DWI measurement allows AxCaliber to tease apart the signals from axons with different diameters. At short diffusion times only small diameter axons exhibit restricted diffusion. As the diffusion time increases, restricted diffusion will be apparent even in larger axons. AxCaliber calculates the estimated signal decay for a series of axon diameters weighted by a diameter distribution function (in previous works we used a γ-distribution). The distribution function is then optimized to provide the best fit to all the signal decay data simultaneously. A full description of the AxCaliber framework is beyond the scope of this paper but is provided in (Assaf *et al*., 2008).

AxCaliber was previously applied to excised nerve tissues (Assaf *et al*., 2006, 2008). In this work, we applied this framework for the *in vivo* measurement of the fibre composition in the corpus callosum. *In vivo* measurements introduce an additional factor—CSF contamination–that is not apparent in excised tissue experiments. To model the partial volume effect of CSF contamination, we added a free diffusing compartment with a fixed diffusion coefficient to the general AxCaliber Equation (Eq. 1).

$$E(q,\Delta) = f_h \cdot E_h(q,\Delta) + f_r \cdot E_h(q,\Delta) + f_{CSF} \cdot E_{CSF}(q,\Delta) \quad (1)$$

Equation (1) describes the contribution of each diffusion compartment to the measured signal decay $E(q,\Delta)$, where f_h and E_h are the respective volume fraction and signal decay of the hindered compartment (extra-axonal space), f_r and E_r are the respective volume fraction and signal decay of the restricted compartment (intra-axonal space), and f_{CSF} and E_{CSF} are the respective volume fraction and signal decay of the CSF compartment. The analytical expressions for E_h and E_r have been described previously. E_{CSF} is modelled using the 1D Stejskal-Tanner equation (Eq. 2):

$$E_{CSF} = \exp(-\gamma^2\delta^2 g^2 D_{CSF}(\Delta - \delta/3)) \quad (2)$$

where γ is the gyro-magnetic ratio, δ is the gradient duration, Δ is the diffusion time and D_{CSF} is the CSF diffusion coefficient (~3 μm^2/ms).

The signal decays obtained at different diffusion times were fitted on a pixel-by-pixel basis simultaneously with AxCaliber (Eq. 1). The ADD appears within the intra-axonal component (E_r) and its weights are given by a gamma function:

$$w_i(a_i;\alpha,\beta) = \frac{a_i^{\alpha-1}e^{-a_i/\beta}}{\beta^\alpha \Gamma(\alpha)} \quad (3)$$

where w_i is the weight for the signal for an axon with diameter a_i. The total number of fitted parameters was five: the volume fraction of the hindered and the CSF components (f_h and f_{CSF}, respectively), the diffusivity of the hindered component (D_h) and parameters of the γ-distribution (α and β). The intra-axonal diffusivity, which was set to 1.4 μm^2/ms.

In order to visualize the ADD pattern along the corpus callosum, we used a clustering algorithm (*k*-means with correlation as the distance measure) with AxCaliber's extracted parameters (D_h, f_h, α and β) used as inputs. Additional information was the spatial location of the voxels which was used only to mark non-adjacent regions with similar ADD into different clusters. The number of clusters (*k*) was incremented until no additional information was observed, and finally was set to seven clusters, one of which was assigned outlier pixels.

Histological analysis

Electron microscopy was performed to estimate the ADD along the corpus callosum by histology. One of the rats was sacrificed and perfused with a paraformaldehyde and glutaraldehyde (50:50) solution. The corpus callosum was isolated and cut into five regions of 1 mm^3. Each region was fixed in 2.5% glutaraldehyde, osmificated, dehydrated with a graded series of ethanol and propylene oxide, and embedded in Araladite solution (Polysciences, Inc., USA). Microsections (70–100 nm) were cut in an ultra-microtome (ultracut S, Reichert, Leica, Sweden). Sections were collected over gelatin slides incubated with a 1% toluidin blue stain for 1 min and examined using a transmission electron microscope (JEM-EX 1200, Jeol, Japan) for analysis. The images were taken with a magnification factor of 15 000.

Analysis of the ADD in the electron microscope images was performed using NIH Image (Bethesda, MD, USA). The axons were selected semi-automatically using threshold segmentation. The threshold (manually adjusted) was used to segment the image into axonal spaces and extra-axonal spaces following which automatic analysis of the area and diameter of each axon could be achieved. The diameter of each axon was estimated from its transverse area. Following this procedure a histogram of the diameter distribution of each region was generated and compared with the measured ADD from AxCaliber analysis.

Statistical analysis

Statistical analysis was done to assess the difference between the corpus callosum clusters found by the *k*-means analysis. Each pixel in each cluster was regarded as an individual observation. The data

were tested for statistical significance using a repeated measure ANOVA with the clusters as the independent factor and the γ-distribution parameters as the repeated variable.

Results

The aim of this work was to extract the ADD from the corpus callosum of the rat brain, *in vivo*, using diffusion MRI measurements. The analysis of the diffusion MRI measurements was done with the AxCaliber framework and is described below. For comparison and validation of the AxCaliber results, the rat brains were removed and prepared for electron microscopy.

Electron microscopy analysis

Figure 1 shows a mid-sagittal T_2-weighted MRI with the corpus callosum outlined. Following the MRI acquisition, the corpus callosum was cut into five segments and a few electron microscopy images (16 images per segment resulting in ~1000 measured axons) were acquired for each segment. A representative image for each section is given in Fig. 1. The extracted axon diameter histograms were measured for each segment (see Methods section) and are depicted below the corresponding electron microscopy image. From the electron microscopy images and histograms, it is obvious that the ADD changes significantly along the corpus callosum, as expected, with narrow distributions at the genu and splenium and much broader distributions in the body of the structure.

AxCaliber and DTI analysis

AxCaliber analysis was performed on a voxel-by-voxel basis providing a set of fitted parameters including: the volume fractions of the CSF compartment, the hindered and restricted component, the diffusivity of the hindered component, and the α and β parameters of the γ-distribution. The γ-distribution is used parametrically to describe the ADD in each voxel. Figure 2 shows a representative dataset for one rat including the different estimate parameters from AxCaliber as well as conventional DTI analysis. Figure 2A shows a mid-saggital T_2-weighted MRI with an inset showing the corpus callosum. Figure 2B and C depict the fractional anisotropy (FA) and the mean apparent diffusion coefficient (ADC) maps extracted from DTI analysis. The f_{CSF} map shows the magnitude of CSF contamination along the corpus callosum (Fig. 2D). The body of the structure has much higher CSF contamination than the genu and splenium, probably due to its smaller volume. The volume fraction of the hindered component was similar along

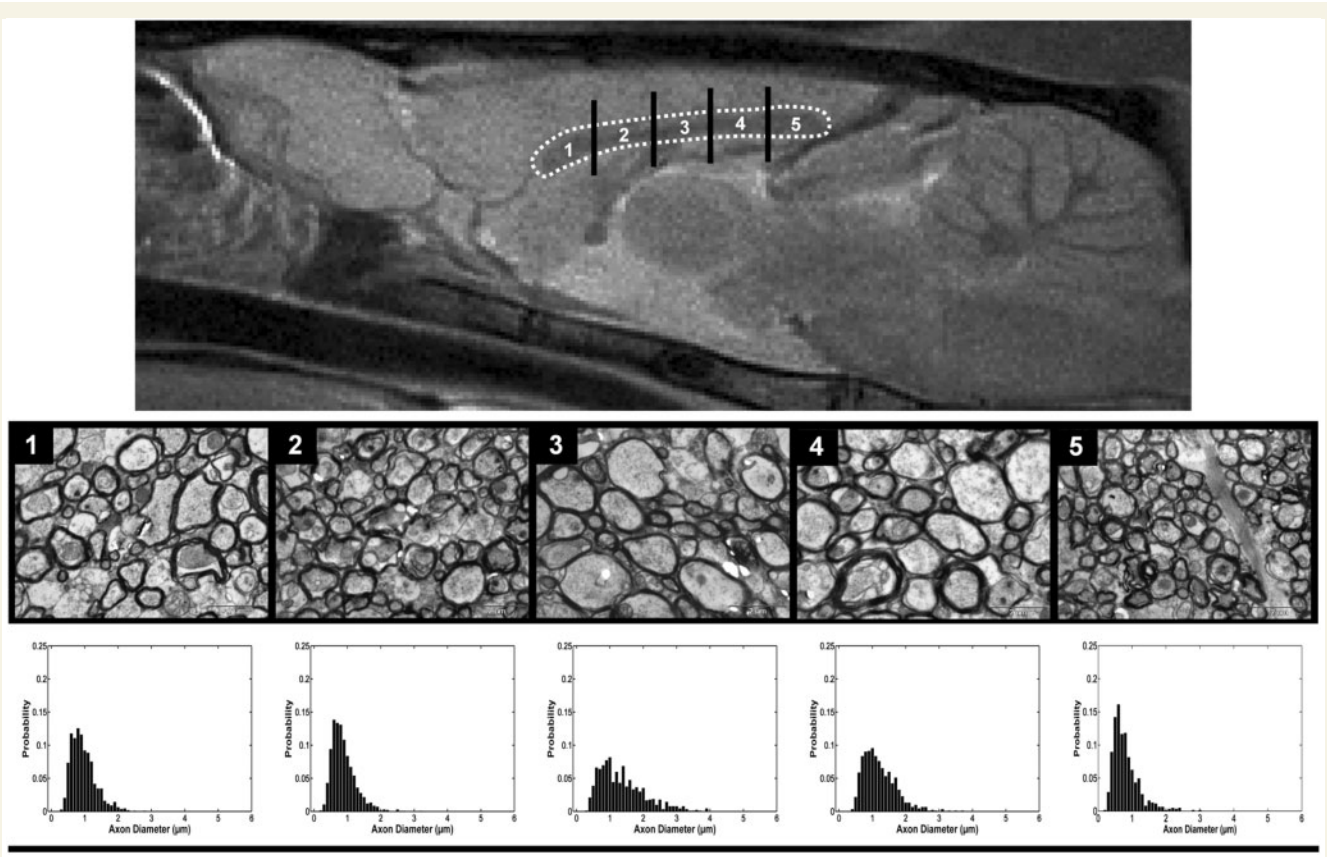

Figure 1 MRI and histological analysis of the corpus callosum. A mid-saggital T_2-weighted MRI of the rat brain with an inset containing the corpus callosum. The corpus callosum is sectioned into five segments from which histological specimens were taken. For each segment a representative electron-microscopy image is given along with the corresponding ADD histogram. Note the difference in ADD along different areas of the structure.

most parts of the area with slightly lower values when approaching the genu (Fig. 2E). The volume fraction of the restricted part changes dramatically along the structure with a much higher volume fraction at the genu and splenium (Fig. 2F) perhaps because these regions are characterized by a higher density of small axons (Fig. 1) and a higher fraction of the axonal compartment. The ADC of the hindered component appears to be uniform along the corpus callosum with a higher diffusivity at its body (Fig. 2G) suggesting that the space between axons may be larger at the body than that at the genu and splenium. Figure 2H and I depict the α and β parameters of the γ-distribution.

To have a better understanding of the meaning of the α and β parameters, we computed the ADD for selected groups of voxels along the corpus callosum that represent each of the five segments (as shown in Fig. 1). Figure 3 shows a mid-saggital T_2-weighted MRI with the region of interest marked in white (2×3 voxels). The computed ADDs for the selected voxels of each region are presented below the image. All the presented ADDs have identical axis proportions/properties, where the *x*-axis represents the mean axon diameter and the *y*-axis is the probability for each diameter. It is clear that the fibre composition within different regions of the corpus callosum is homogeneous—most of the voxels at its genu and splenium have a narrow distribution while the voxels at the body have a much broader distribution.

Clustering analysis

To visualize the difference in the computed ADD without the need to explore the γ-function for each voxel, we used cluster analysis to segment the corpus callosum based on the ADD parameters. The cluster analysis for a representative rat is shown in Fig. 4A (inset shown in Fig. 4B). Seven clusters were input, one of which represented noise or partial volume at the edges of the corpus callosum. The remaining six clusters represented five segments of the structure (i.e. two clusters were merged). The red, brown and orange clusters in Fig. 4 correspond to the genu, the blue and cyan clusters correspond to the body and edge of the splenium, and the light green cluster corresponds to the splenium. The computed AxCaliber ADDs are shown for the five segments in Fig. 4C. The AxCaliber and electron microscopy ADDs (as shown in Fig. 1) show good agreement: a narrow distribution in the genu and splenium, and a much broader distribution in the body. It should also be noted that the means of the AxCaliber ADDs are slightly higher than those of the electron microscopy distribution. Figure 5 shows cluster analysis for three different rats that segment the corpus callosum into five distinct areas. The clusters as well as the measured AxCaliber parameters such as the computed ADDs in each cluster (data not shown) were similar in all rats.

Correlation between AxCaliber parameters and DTI indices

We also performed a correlation analysis between DTI and AxCaliber derived parameters (Fig. 6). In general, the extracted ADD from AxCaliber did not correlate well with any DTI indices (ADC, FA and axial and radial diffusivities in Fig. 6B, respectively). The ADD had a negative correlation with all parameters except for the radial diffusivity where a positive correlation was found. Interestingly, the highest and most significant correlation was found between the mean diameter obtained from the ADD and

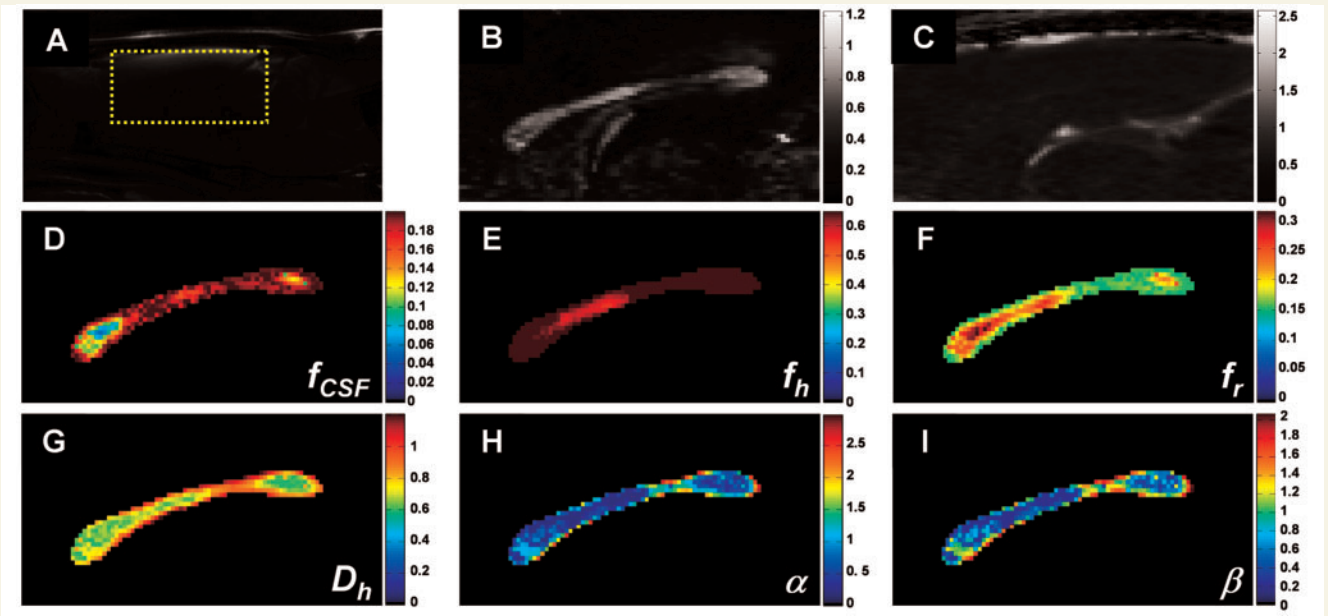

Figure 2 AxCaliber analysis of the rat corpus callosum. (**A**) A mid-saggital T_2-weighted MRI with an inset containing the ROI (**B**) and (**C**) FA and mean ADC maps of the same slice in (**A**) computed from DTI dataset. (**D–F**) The volume fractions of each of the AxCaliber components: CSF (**D**), hindered (**E**) and restricted/axonal (**F**). (**G**) Map of the ADC of the hindered component of AxCaliber. (**H** and **I**) Maps of the α and β parameters of the γ-distribution representing the computed ADD.

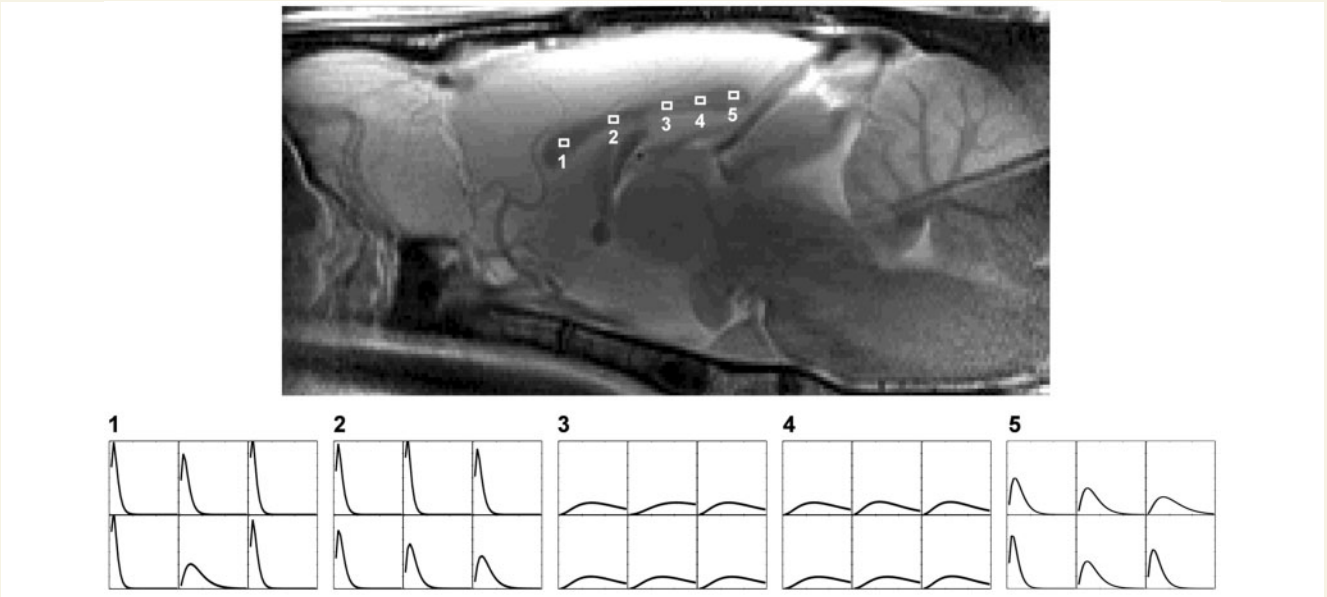

Figure 3 Axon diameter distribution analysis along the corpus callosum. A mid-saggital T_2-weighted MRI with five regions of interest outlined representing the five segments shown in Fig. 1. Each region was consisted of 2×3 voxels. The computed ADD from AxCaliber for each voxel within each region is depicted at the bottom. Note the homogenous pattern of ADD within each region and the large differences between them. All ADDs are in the same proportion, the *x*-axis represents the axon diameters (from 0 to 6 μm) and the y-axis represents the probability (from 0 to 0.3).

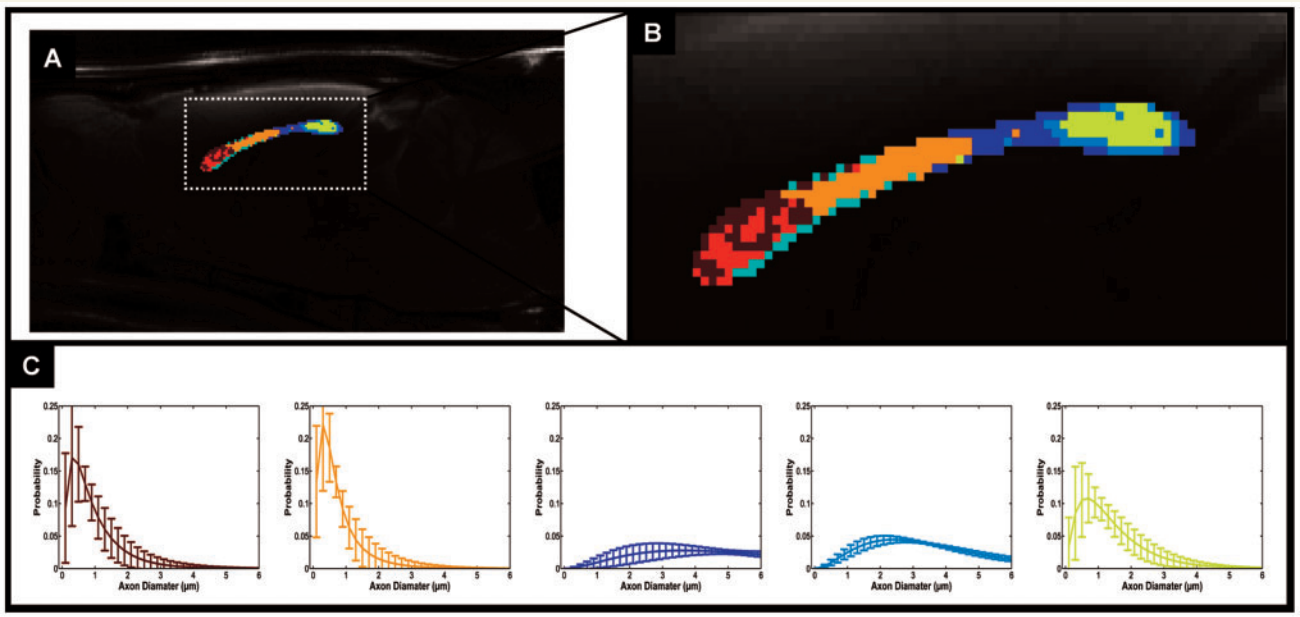

Figure 4 Cluster analysis of the axon diameter distribution along the corpus callosum. (**A**) A mid-saggital T_2-weighted MRI with the AxCaliber clusters superimposed, enlarged at (**B**). (**C**) The AxCaliber averaged ADDs for the different clusters given in (**A**) and (**B**); note that the colours of the graphs match the clusters' colours.

the axial diffusivity ($R^2 = 0.33$, $P < 0.0001$). Indeed, the axial diffusivity and FA maps (third and second images in Fig. 6A, respectively) can be visually divided into the different segments of the corpus callosum. This might be a result of CSF contamination that has the same pattern (Fig. 2D). The weakest correlation was found between the ADC and mean ADD. In addition, the graphs show the limitation of AxCaliber as it could not extract mean axon diameters smaller than 0.4 μm indicated by the floor effect (Fig. 6).

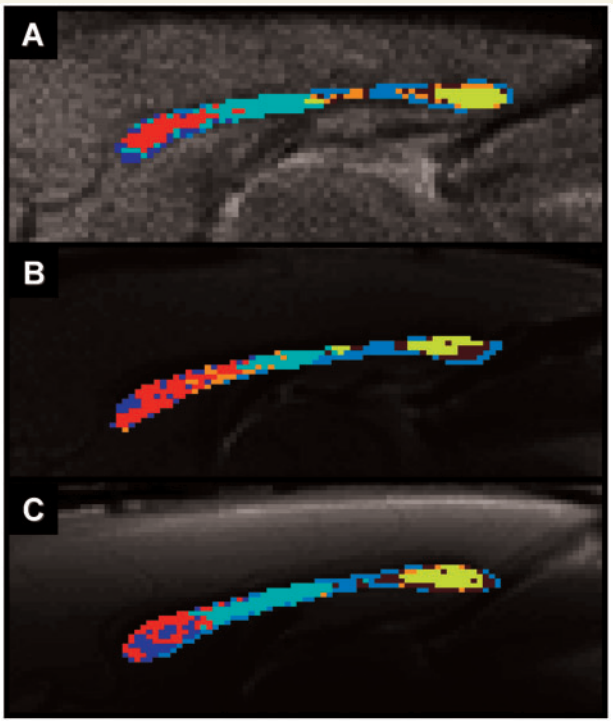

Figure 5 Cluster analysis of the axon diameter distribution for different rats (**A–C**). A mid-saggital T_2-weighted MRI with the AxCaliber cluster superimposed for three different rats. Note that the colours of the clusters for the three rats are matched. Also note the high similarity of the cluster pattern among the rats.

Discussion

This article reports the first *in vivo* measurement of the ADD based on the diffusion/displacement properties of water molecules in white matter demonstrated on the rat's corpus callosum. Conventional measurement of the ADD requires sacrificing the animal and excising, fixing, sectioning, staining and image processing only a small portion of the tissue sample. The ability to obtain the ADD, *in vivo*, within each image pixel turns MRI into a virtual microscope.

AxCaliber has all the advantages of other MRI based methodologies, especially speed and non-invasiveness. In particular, as a tool for measuring the ADD, it allows one to probe large tissue regions without being a propensity to histological preparation artifacts. It should be noted, however, that this methodology has some of the limitations that affect any other diffusion MRI based method. As a diffusion based framework, AxCaliber is limited in the range of experimental diffusion times and length scales that it can probe (see limitations below). A specific limitation of AxCaliber, in its present form, is the need to observe displacements exactly perpendicular to the fibre direction.

AxCaliber measures a morphological parameter of the tissue, the ADD. However, it is a known concept in neuroscience that morphology and function are linked therefore the ability to estimate or measure fine morphological features may imply on the functionality of the tissue. Using this concept, AxCaliber may help to advance our knowledge on the functional deficits that occur in various brain diseases and disorders.

Validation of AxCaliber

AxCaliber has already been tested and validated using a number of means (Assaf *et al*., 2006, 2008). First, we subjected the method to synthetic datasets in which we generated mathematical axons with a known parametric ADD (Assaf *et al*., 2006, 2008). We then used the AxCaliber modelling framework to estimate or infer the ADD from these synthetic tissue specimen. Moreover, we have used AxCaliber to estimate the ADD within fixed porcine spinal cord, optic nerve and sciatic nerve specimens and then compared these findings to those obtained with histology using a variety of myelin and tissue staining techniques (Assaf *et al*., 2008).

For a fixed specimen, histological analysis provides the ground truth for validating the AxCaliber ADD. However, *in vivo*, the situation is more complicated. In general, good agreement was found between the AxCaliber and electron microscopy ADDs. However, we consistently observe that the mean ADD using AxCaliber is larger than the mean ADD obtained from histological analysis. It should be noted that tissue shrinkage is seen as a possible confound in the histological preparation of neural tissue (Virtanen *et al*., 1984). This result is not surprising because the dehydrating effect of formaldehyde and its specific interactions with macromolecules comprising the neural tissue could easily explain the reduction in tissue volume and axon diameter. Moreover, in previous work where AxCaliber was validated on excised and fixed tissue the histological and AxCaliber ADDs did not differ significantly (Assaf *et al*., 2008). This implies that the shift of the ADD to larger values in the *in vivo* experiment can be explained by the histological shrinkage effect and not computational or model artifact.

In addition to the ADD, AxCaliber extracts other parameters such as the fractional volume of each compartment (Fig. 2D–F). The volume fraction of the axonal compartment is estimated at ~20% with AxCaliber (Fig. 2F) while histological analysis reveals much higher fraction. It should be noted that these are only relative fractions and are weighted by the MRI T1 and T2 relaxation times which may be different for each compartment. This could explain the discrepancy between the MRI and histological volume fractions.

MRI of the corpus callosum

Various MRI methods have been used to image the corpus callosum (Georgy *et al*., 1993; Uchino *et al*., 2006). High resolution T1 MRIs show significant contrast between grey and white matter, but are inherently insensitive to white matter microstructure and micro-architecture. Magnetization Transfer MRI is dependent not only on myelin content, but also on many other factors, making it both non-specific and non-quantitative in relation to the ADD. DTI provides various measures of diffusion anisotropy that are useful in depicting white matter (Basser *et al*., 1994; Basser, 1995; Pierpaoli and Basser, 1996; Pierpaoli *et al*., 1996; Basser and

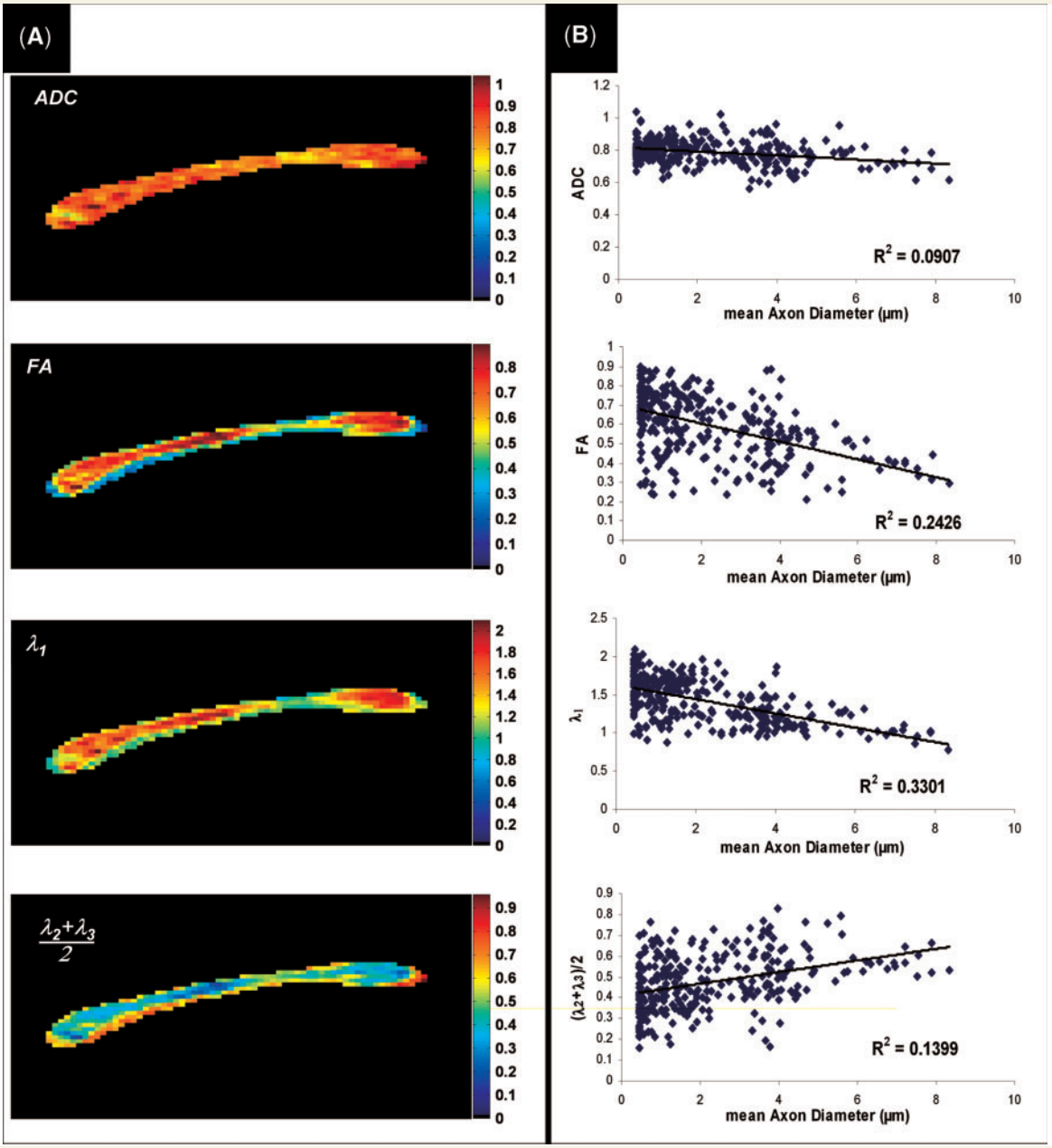

Figure 6 Comparison of AxCaliber with DTI. (**A**) The indexed DTI maps of the ADC, FA and longitudinal (λ_1) and radial diffusivities [$(\lambda_2+\lambda_3)/2$] of the same rat shown in Figs 1–3. (**B**) Correlation between each of the DTI indices and AxCaliber's mean axon diameter (averaged from the computed ADD). Note that the correlations are relatively poor. The statistical significance in correlations was $P<0.00001$).

Pierpaoli, 1998; Basser and Jones, 2002). These anisotropy measures, however, are sensitive to many micro-structural features of white matter, such as ADD, the axon population fraction or density, the orientation distribution of axons, and the degree of myelination (Pierpaoli *et al*., 1996; Song *et al*., 2005; Sun *et al*., 2006; Budde *et al*., 2007; Assaf and Pasternak, 2008). Therefore, FA and other similar parameters are non-specifically related to axon composition and micro-architecture although they are affected by them (Fig. 6). The ADC in normal brain parenchyma is so uniform that it is often difficult to distinguish between grey and white matter. We performed a correlation between the different DTI indices and the mean axon diameters (as extracted from AxCaliber) on a voxel-by-voxel basis (Fig. 6). Indeed a weak correlation was found between them where the weakest correlation is with the ADC and the strongest is with axial diffusivity. We found that the radial diffusivity was positively correlated with the mean axon diameter while the axial diffusivity was negatively correlated with it. It can be speculated that small mean axon diameter will lead to high axonal density and thus to overall reduced radial diffusivity, hence a positive correlation between these parameters

is expected. Concomitantly, high packing of the axons causes high tension (or stretching) of the fibres, which in turn increases the axial diffusivity (i.e. less disturbances to diffusion along the fibres), hence negative correlation between the two parameters is expected. On the other hand, one cannot rule out the effect of CSF contamination on the axial diffusivity since it is more prominent in regions of broad ADD (Fig. 3D). Finally, although some correlation between the DTI indices and the axon diameter is present (Fig. 6), the relationship between the two parameters is not straightforward.

Currently, no other existing MRI methodology can provide specific anatomical or microstructural information about packs of axons, as AxCaliber does. Previous works tried to use geometrical models of diffusion in white matter to extract the mean axon diameter (but not the distribution) (Stanisz *et al*., 1997). Such approaches found good correlation between the histological measures and the model estimations (Stanisz *et al*., 1997; Ong *et al*., 2008). Other works tried to use the q-space approach to estimate the displacement distribution function from which the mean axon size can be calculated (Assaf *et al*., 2002*b*; Ong *et al*., 2008). In general the q-space analysis provides a better estimation of the axonal compartment than regular DTI but as noted above does not directly measure the ADD (Assaf *et al*., 2002*a*). Moreover, the pattern of the ADDs along the corpus callosum fits its known anatomical and functional organization. While regions that need fast and efficient transmission are characterized by broad distribution, other areas have much narrower distributions centered on small diameter values (Aboitiz *et al*., 1992; Olivares *et al*., 2000; Olivares *et al*., 2001; Aboitiz and Montiel, 2003).

Applications of AxCaliber

Applications of AxCaliber are expected to be widespread. Little is currently known about the change in the ADD in normal and abnormal development. AxCaliber provides a new tool for such developmental studies (on a large population), since its non-invasive character provides opportunities to follow changes in ADD longitudinally. In the clinic, one can anticipate many diagnostic uses in neuroradiology and neurology. Many disorders including neuritis, MS, ALS and Guillain-Barre may result in changes in ADD. It is reasonable to speculate that there are applications in psychiatry where the ADD may be implicated in a number of cognitive and behavioural disorders, disconnection syndromes and psychiatric conditions (e.g. schizophrenia). The ADD, because of its intimate connection with the information carrying capacity and signal latency in white matter pathways, is expected to play an important role in normal brain function, particularly in mediating communication between different brain regions. Therefore, deviations from normal ADDs may provide an anatomical substrate for many disorders. The ADD could also be useful in monitoring the efficacy of the various regenerative (e.g. stem cell) and gene therapies as well as in assessing the effectiveness of different neuroprotective or psychiatric drugs. It could also be used to follow the effects of different endogenous chemicals, such as hormones, growth factors, tissue necrosis factors, etc. This approach could be also used to assess the effect of different genes on the nervous system in knock-out or knock-in studies. In the neurosciences AxCaliber could be used to estimate information transfer and processing limits along different white matter pathways, leading to a better understanding of information flow and transfer in the nervous system overall. It is reasonable to speculate that AxCaliber could be used to study nerve routes from the spinal cord as well as a variety of peripheral nerve bundles, such as the sciatic nerve and radial nerve.

The basis of AxCaliber is the differentiation between two modes of diffusion: hindered and restricted. In AxCaliber the restricted diffusion component is represented by a set of cylinders with variable sizes. In a similar manner, it is possible to define a model of diffusion within spheres that will be able to infer the microstructure features of grey matter extracting parameters such as cell size distribution and cellular density. However, a model of diffusion in grey matter should include additional factors to account for exchange between the different compartments.

Limitations

AxCaliber is subject to a number of limitations. It is based on a model of intra- and extra-axonal diffusion (CHARMED), which may or may not apply in all white matter regions, where for instance, compartmental exchange may be important. In addition, this model assumes that the diffusion gradients applied are orthogonal to the axon fibre axis, although it can be generalized to three dimensions. However, a 3D AxCaliber acquisition and analysis might be too computationally taxing to be practically feasible. The corpus callosum is the best fibre system to test AxCaliber due to its ordered alignment and thickness; however, applying the methodology on other fibre systems is possible by knowing *a priori* the path of the fibres (e.g. from DTI based tractography). This procedure, however, will require additional development of the methodology. One option is to acquire the multi diffusion time dataset using several gradient directions and estimate, based on the eigen-vectors derived from DTI analysis, the signal decay as if it were measured perpendicular to the fibres. It should be noted that such modification will not be valid in areas where fibres kiss, cross, twist or splay. AxCaliber also uses a parametric statistical distribution for the ADD—a γ-distribution—which might not be appropriate for pathological conditions. In this case, the ADD could be estimated using a non-parametric procedure (Assaf and Basser, 2007). The limitations in the ability to apply short pulsed field gradients or long diffusion times limits the ultimate range of diameters one can probe with this technique (Mitra and Halperin, 1995; Codd and Callaghan, 1999). For example, Fig. 6 shows that the smallest axon diameter that could be extracted was only $\sim$0.4 μm, which lead to the floor effect of the ADD. This is a result of the maximal q value used in the experiment that can not probe smaller displacements.

AxCaliber can be applied clinically without much modification to the MRI pulse sequences used in this rat brain study. One must appropriately account for the 'fat' or long-duration pulsed field gradients used to obtain diffusion weighted image data and function within the limitations of gradient strength imposed by the scanner hardware (Codd and Callaghan, 1999). New methods to account for the effect of 'fat pulses' have already been developed

for this purpose, and must be used to interpret data obtained using conventional clinical DWI sequences.

Conclusions

As function and anatomy are strongly linked in the nervous system, the ADD is clearly an important anatomical parameter that affects key functional properties of nerves and nerve pathways. Because of the inability, to date, to measure this parameter non-invasively and *in vivo*, little is known about its changes in normal and abnormal development; its alterations in aging; degeneration and disease; and its effect on brain function. We believe that the advent of AxCaliber, and its use on the corpus callosum and eventually in other pathways in the CNS and PNS, will advance many practical clinical applications as well as our understanding of the function of the nervous system.

Acknowledgements

The authors wish to thank Tamar Blumenfled-Katzir for help in histological analysis. The authors also wish to thank the Israel Science Foundation and the Raymond and Beverly Sackler Institute for Biophysics of Tel Aviv University for purchasing the MRI scanner and to the Strauss Institute for Computational Imaging of Tel Aviv University.

Funding

Intramural Research Program of the Eunice Kennedy Shriver National Institute of Child Health and Human Development (to P.J.B.); National Institutes of Health (to P.J.B.). The Israel Science Foundation grant no. 994/08 (to Y.A.).

References

Aboitiz F, Montiel J. One hundred million years of interhemispheric communication: the history of the corpus callosum. Braz J Med Biol Res 2003; 36: 409–20.

Aboitiz F, Scheibel AB, Fisher RS, Zaidel E. Fiber composition of the human corpus callosum. Brain Res 1992; 598: 143–53.

Assaf Y, Basser PJ. Composite hindered and restricted model of diffusion (CHARMED) MR imaging of the human brain. Neuroimage 2005; 27: 48–58.

Assaf Y, Basser PJ. Non parametric approach for axon diameter distribution estimation from diffusion measurements. Proc Intl Soc Magn Reson Med 2007; 15: 1536.

Assaf Y, Ben-Bashat D, Chapman J, Peled S, Biton IE, Kafri M, et al. High b-value q-space analyzed diffusion-weighted MRI: application to multiple sclerosis. Magn Reson Med 2002a; 47: 115–26.

Assaf Y, Blumenfeld-Katzir T, Yovel Y, Basser PJ. AxCaliber: a method for measuring axon diameter distribution from diffusion MRI. Magn Reson Med 2008; 59: 1347–54.

Assaf Y, Blumenfeld T, Levin G, Yovel Y, Basser PJ. AxCaliber – a method to measure the axon diameter distribution and density in neuronal tissues. Proc Intl Soc Magn Reson Med 2006; 14: 637.

Assaf Y, Freidlin RZ, Rohde GK, Basser PJ. New modeling and experimental framework to characterize hindered and restricted water diffusion in brain white matter. Magn Reson Med 2004; 52: 965–78.

Assaf Y, Kafri M, Shinar H, Chapman J, Korczyn AD, Navon G, et al. Changes in axonal morphology in experimental autoimmune neuritis as studied by high b-value q-space (1)H and (2)H DQF diffusion magnetic resonance spectroscopy. Magn Reson Med 2002b; 48: 71–81.

Assaf Y, Pasternak O. Diffusion tensor imaging (DTI)-based white matter mapping in brain research: a review. J Mol Neurosci 2008; 34: 51–61.

Basser PJ. Inferring microstructural features and the physiological state of tissues from diffusion-weighted images. NMR Biomed 1995; 8: 333–44.

Basser PJ, Jones DK. Diffusion-tensor MRI: theory, experimental design and data analysis - a technical review. NMR Biomed 2002; 15: 456–67.

Basser PJ, Mattiello J, LeBihan D. MR diffusion tensor spectroscopy and imaging. Biophys J 1994; 66: 259–67.

Basser PJ, Pierpaoli C. A simplified method to measure the diffusion tensor from seven MR images. Magn Reson Med 1998; 39: 928–34.

Budde MD, Kim JH, Liang HF, Schmidt RE, Russell JH, Cross AH, et al. Toward accurate diagnosis of white matter pathology using diffusion tensor imaging. Magn Reson Med 2007; 57: 688–95.

Codd SL, Callaghan PT. Spin echo analysis of restricted diffusion under generalized gradient waveforms: planar, cylindrical, and spherical pores with wall relaxivity. J Magn Reson 1999; 137: 358–72.

Georgy BA, Hesselink JR, Jernigan TL. MR imaging of the corpus callosum. AJR Am J Roentgenol 1993; 160: 949–55.

Hughes JR. Autism: the first firm finding = underconnectivity? Epilepsy Behav 2007; 11: 20–4.

Hursh JB. The properties of growing nerve fibers. Am J Physiol 1939; 127: 140–53.

Kamnasaran D. Agenesis of the corpus callosum: lessons from humans and mice. Clin Invest Med 2005; 28: 267–82.

Livy DJ, Elberger AJ. Alcohol exposure during the first two trimesters-equivalent alters the development of corpus callosum projection neurons in the rat. Alcohol 2008; 42: 285–93.

Mitra PP, Halperin BI. Effects of finite gradient-pulse widths in pulsed-field-gradient diffusion measurements. J Magn Reson Ser A 1995; 113: 94.

Njiokiktjien C, de Sonneville L, Vaal J. Callosal size in children with learning disabilities. Behav Brain Res 1994; 64: 213–8.

Olivares R, Michalland S, Aboitiz F. Cross-species and intraspecies morphometric analysis of the corpus callosum. Brain Behav Evol 2000; 55: 37–43.

Olivares R, Montiel J, Aboitiz F. Species differences and similarities in the fine structure of the mammalian corpus callosum. Brain Behav Evol 2001; 57: 98–105.

Ong HH, Wright AC, Wehrli SL, Souza A, Schwartz ED, Hwang SN, et al. Indirect measurement of regional axon diameter in excised mouse spinal cord with q-space imaging: simulation and experimental studies. Neuroimage 2008; 40: 1619–32.

Pierpaoli C, Basser PJ. Toward a quantitative assessment of diffusion anisotropy. Magn Reson Med 1996; 36: 893–906.

Pierpaoli C, Jezzard P, Basser PJ, Barnett A, Di Chiro G. Diffusion tensor MR imaging of the human brain. Radiology 1996; 201: 637–48.

Piven J, Bailey J, Ranson BJ, Arndt S. An MRI study of the corpus callosum in autism. Am J Psychiatry 1997; 154: 1051–6.

Randall PL. Schizophrenia, abnormal connection, and brain evolution. Med Hypotheses 1983; 10: 247–80.

Rice D, Barone S Jr. Critical periods of vulnerability for the developing nervous system: evidence from humans and animal models. Environ Health Perspect 2000; 108 (Suppl 3): 511–33.

Ritchie JM. On the relation between fibre diameter and conduction velocity in myelinated nerve fibres. Proc R Soc Lond B Biol Sci 1982; 217: 29–35.

Song SK, Yoshino J, Le TQ, Lin SJ, Sun SW, Cross AH, et al. Demyelination increases radial diffusivity in corpus callosum of mouse brain. Neuroimage 2005; 26: 132–40.

Stanisz GJ, Szafer A, Wright GA, Henkelman RM. An analytical model of restricted diffusion in bovine optic nerve. Magn Reson Med 1997; 37: 103–11.

Sun SW, Liang HF, Trinkaus K, Cross AH, Armstrong RC, Song SK. Noninvasive detection of cuprizone induced axonal damage and demyelination in the mouse corpus callosum. Magn Reson Med 2006; 55: 302–8.

Tasaki I, Ishii K, Ito H. On the relation between the conduction-rate, the fiber-diameter and the internodal distance of the medullated nerve fiber. Jpn J Med Sci III, Biophysics 1943; 9: 189–99.

Uchino A, Takase Y, Nomiyama K, Egashira R, Kudo S. Acquired lesions of the corpus callosum: MR imaging. Eur Radiol 2006; 16: 905–14.

Virtanen J, Uusitalo H, Palkama A, Kaufman H. The effect of fixation on corneal endothelial cell dimensions and morphology in scanning electron microscopy. Acta Ophthalmol (Copenh) 1984; 62: 577–85.

Waxman SG. Determinants of conduction velocity in myelinated nerve fibers. Muscle Nerve 1980; 3: 141–50.

Waxman SG, Kocsis JD, Stys PK. The axon: structure, function, and pathophysiology. New York: Oxford University Press; 1995.